Article

pubs.acs.org/Biomac

Chain Flexibility and Dynamics of Polysaccharide Hyaluronan in Entangled Solutions: A High Frequency Rheology and Diffusing Wave Spectroscopy Study

C. Oelschlaeger,* M. Cota Pinto Coelho, and N. Willenbacher

Institute for Mechanical Process Engineering and Mechanics, Karlsruhe Institute of Technology (KIT), 76131 Karlsruhe, Germany

ABSTRACT: We have investigated the linear viscoelastic properties of high molecular weight hyaluronan in aqueous solution using an experimental approach combining mechanical rheometry and optical microrheology. The complex shear modulus has been measured over a broad frequency range from 10^{-1} to 10^{7} rad/s. Chain flexibility is characterized by the persistence length $l_p$and this parameter has been determined for the first time in the entangled regime here from high frequency modulus data. At NaHA concentrations above the entanglement concentration c_e, l_p is essentially independent of polymer concentration, temperature, and ionic strength. The latter is consistent with the Odijk−Skolnick−Fixman theory. The scaling exponent describing the concentration dependence of the plateau modulus G_0 agrees well with predictions for polymers in good solvents. The scaling exponents for the specific viscosity η_{sp} and relaxation time T_R are slightly higher than theoretically predicted for polyelectrolytes in the high salt limit, indicating, that molecular aggregation occurs at higher polymer concentrations.

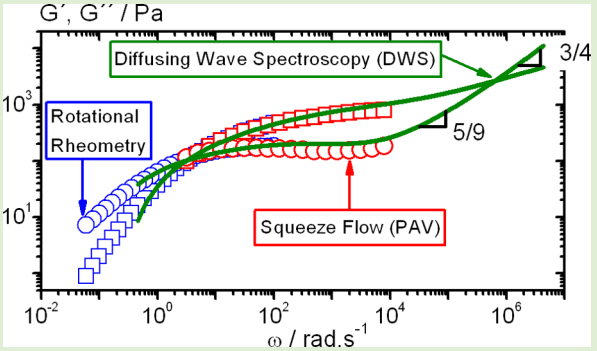

INTRODUCTION

Hyaluronan, also known as sodium hyaluronate (NaHA) is a linear polysaccharide composed of repeating disaccharide units of *N*-acetyl glucosamine and glucuronate (linked by β 1−3 and β 1−4 glycosidic bonds) and counterions. It is used in cell culture, medical devices, pharmaceutical applications such as eye drops, viscoelastic devices, and drug delivery. NaHA is found in large quantities in animals and the human body, where it is mainly produced by fibroblasts and other specialized tissues cells. In this study, NaHA has been produced from bacteria fermentation, which provides a product without animal-derived raw materials and of high degree of purity. Many rheological[1−4] and conformational[5,6] studies have been performed on NaHA in both the dilute and the semidilute regime. This latter concentration region is of particular relevance, because in natural biological conditions NaHA molecules are in a crowded environment, including other macromolecules. Additionally, in this regime, recent light scattering measurements[7] have shown the existence of NaHA associations or microgels probably due to interchain hydrogen bonds. These hydrogen bonds are very important because they control the local stiffness of the polymer, reflected by its intrinsic persistence length, l_p. In the literature, discordant values of l_p, mainly in the dilute regime, are reported. Some experimental data based on scattering and intrinsic viscosity measurements suggest a moderate stiffness, that is, l_p of about 4−5 nm.[5,8−11] Other authors[1,12−15] have found higher l_p values varying between 8 and 10 nm at high ionic strength and for 1 mM added NaCl a l_p value of almost 40 nm is reported.[16] More recently, Buhler et al.[17,18] and Esquenet et al.[7] by static, dynamic, and small-angle neutron scattering measure values for the persistence length of about 8−9 nm and suggests that the total persistence length is almost doubled in conditions of low ionic strength due to the electrostatic contribution. These latter experimental values are in good agreement with theoretical persistence length values (l_p = 7.5 nm) obtained from molecular modeling.[19] Hyaluronan can be considered as a polyelectrolyte and in that case the total persistence length is written as

$$l_{p,T} = l_{p,0} + l_{p,e} \quad (1)$$

$l_{p,T}$ is the sum of two contributions: the intrinsic persistence length $l_{p,0}$ due to the rigidity of the uncharged chain and the electrostatic persistence length $l_{p,e}$ arising from the repulsions between neighbor ionic sites. For polysaccharides the electrostatic contribution is usually much smaller than the intrinsic contribution. Assuming a Debye−Hückel potential and under the condition that cation condensation occurs,[20] Odijk,[21] Skolnick and Fixman[22] have derived a relation given $l_{p,e}$:

$$l_{p,e} = \frac{\xi^2}{4\kappa^2 l_B} \quad \text{for} \quad \xi < 1 (\text{OSF relation}) \quad (2)$$

where l_B is the Bjerrum length (0.713 nm in water) and κ^{-1} the Debye−Hückel screening length related to the concentration of

Received: July 18, 2013
Revised: August 26, 2013

   dx.doi.org/10.1021/bm4010436 | *Biomacromolecules* XXXX, XXX, XXX−XXX

the counterions. The structural charge parameter ξ is defined as the ratio of l_B and a distance between two adjacent ionic sites. For hyaluronan a = 1.02 nm and, hence, ξ = 0.7.[17] In that case counterion condensation is not of relevance. Additionally, in dilute polyelectrolyte solutions

$$\kappa^2 = 4\pi l_B c_f \quad \text{with} \quad c_f = c + 2c_s \tag{3}$$

c_f is the concentration of free monovalent ions, c is the polymer concentration, and c_s is the excess salt concentration.

In the present study, we have used for the first time a combined experimental approach[23] using mechanical high frequency rheology and optical microrheology to determine the linear viscoelastic properties of polysaccharide solutions in the frequency range from 10^{-1} up to 10^7 rad/s. In the high frequency regime, the stress relaxation is controlled by the internal dynamics of individual molecules and the moduli G' and G'' show characteristic scaling behavior:

$$G' \sim G'' \sim \omega^{\alpha} \tag{4}$$

First the Rouse-Zimm modes dominate and α = 1/2−2/3. At even higher frequencies internal bending modes of single Kuhn segments determine G' and G'', and hence, these dynamic parameters are related to the bending modulus β, often expressed in terms of the persistence length through $\beta = k_B \cdot T \cdot l_p$. In this frequency range, the scaling exponent α = 3/4, as predicted by Morse[24] and Gittes and MacKintosh.[25] The transition between these scaling regimes is marked by the inverse of the shortest Rouse relaxation time $\omega_0 = \tau_0^{-1}$, which is directly related to the persistence length l_p:

$$\omega_0 = \frac{k_B T}{8\eta_s l_p} \tag{5}$$

where η_s is the solvent viscosity.

The persistence length $l_p$can also be determined from the absolute values of G' and G'' in the α = 3/4 scaling regime from a relationship based on a statistical mechanical treatment of the single filament stress response of semi flexible chains:[25]

$$G^* = \frac{\rho}{15}\kappa l_p \left(\frac{-2i\zeta}{\kappa}\right)^{3/4} \omega^{3/4} - i\omega\eta_s \tag{6}$$

where ζ is the lateral drag coefficient and ρ the area density of polymers. The latter can be calculated as $\rho = \varphi_{poly}/((\pi/4)d^2)$, where φ_{poly} is the polymer concentration (v/v) and $((\pi/4)d^2)$ is the cross-sectional area of the polymer.

In this study, we characterize the linear viscoelastic properties of hyaluronan solutions in the entangled semidilute regime using diffusing wave spectroscopy (DWS) based tracer microrheology as well as various mechanical techniques such as rotational rheometry and oscillatory squeeze flow covering the frequency range from 10^{-1} to 10^7 rad·s^{-1}. We determine for the first time the persistence length l_p of hyaluronan solutions directly from high frequency rheological measurements either by determination of ω_0 or from absolute values of G^* in the frequency range $\omega \gg \omega_0$. Variation of l_p with NaHA concentration, ionic strength, and temperature is investigated. Another key structural parameter for polysaccharide solutions investigated here is the plateau modulus G_0. This parameter, determined at intermediate frequencies, is directly related to the mesh-size λ of the system with $G_0 \sim \lambda^{-3}$. So far, G_0 of NaHA has been determined from the relation $\eta_0 = G_0 \cdot T_R$[26] or from master curves of G' and G''.[27] Here, for the first time, we measure G_0 directly and investigate its dependence on hyaluronan concentration in a large concentration range. We also determine the specific viscosity η_{sp} and relaxation time T_R and establish for each parameter the scaling laws to dilution and compare results with scaling predictions for polyelectrolytes in the high salt limit[28] and neutral polymer in good solvent.[29] Variations of those parameters with temperature and ionic strength are also investigated. Table 1 below gives predictions for both semidilute unentangled and entangled solutions.

Table 1. Scaling Predictions for Polyelectrolytes in the High Salt Limit[28] and Neutral Polymer in Good Solvent[29] for Both Semidilute Unentangled and Entangled Solutions

	unentangled semidilute polyelectrolyte in high salt	entangled semidilute polyelectrolyte in high salt and neutral polymer in good solvent
specific viscosity: η_{sp}	$c^{1.25}$	$c^{3.75}$
relaxation time: T_R	$c^{0.25}$	$c^{1.5}$
plateau modulus: G_0		$c^{2.25}$

EXPERIMENTAL SECTION

Sample Characteristics. Hyaluronan, also called sodium hyaluronate (NaHA), used in this work was donated by Novozymes Biopharma (Bagsvaerd, Denmark) and is sold under the commercial name Hyasis (molecular weigth $M_w = 1.43 \times 10^6$ g/mol determined by SEC-MALS). The production method is based on fermentation of the safe bacterial strain *Bacillus subtilis*. This method allows to achieve a high degree of purity; the process uses minimal media, no animal-derived raw materials, and a proprietary water-based technology that eliminates the use of organic solvents. The polydispersity is equal to 1.4, the mass of a monomer unit is 400 g/mol, the length of a monomer is 1.02 nm, and the weight-averaged contour length is equal to L_c = 3.6 μm. NaHA aqueous solutions were investigated in the polymer concentration range from 1 to 50 g/L, that is, in the semidilute regime, at different temperatures (20, 40, and 60 °C) and in presence of NaCl.

DWS Based Optical Microrheology. DWS uses the equilibrium thermal response of small (colloidal) particles embedded in a material to obtain quantitative information about the macroscopic loss and storage moduli, $G'(\omega)$ and $G''(\omega)$, over an extended range of frequencies. This is based on a quantitative relationship between the tracer mean-squared displacement $\langle \Delta r^2(t) \rangle$ and the complex shear modulus $G^*(\omega) = G'(\omega) + iG''(\omega)$.[30] The Laplace transform of the particle mean squared displacement $\langle \Delta \tilde{r}^2(i\omega) \rangle$ is related to the complex modulus of the sample via a generalized Stokes−Einstein equation (GSE):

$$G^*(\omega) = \frac{k_B T}{\pi a \cdot i\omega \langle \Delta \tilde{r}^2(i\omega) \rangle} = G'(\omega) + iG''(\omega) \tag{7}$$

For a quantitative interpretation of the raw experimental data $\langle \Delta r^2(t) \rangle$ the Laplace transformation is the most critical part of the analysis. To reduce truncation errors we apply a procedure suggested by Mason et al.[31] and $\tilde{G}(S)$ is estimated by substituting $\langle \Delta r^2(t) \rangle$ into an algebraic Stokes- Einstein form:[32]

$$\tilde{G}(s) = \left. \frac{k_B T}{\pi a \langle \Delta r^2(t) \rangle \Gamma[1 + (\partial \ln \langle \Delta r^2(t) \rangle / \partial t)]} \right|_{t=1/s} \tag{8}$$

To reduce scatter, we first fit $\langle \Delta r^2(t) \rangle$ with a polynomial of order 6 or 7 and then use eq 7 to extract the moduli $G'(\omega)$ and $G''(\omega)$. The choice of the polynomial order and the range of data selected do not influence the results significantly.[23] At times shorter than 10^{-5} s, or

dx.doi.org/10.1021/bm4010436 | Biomacromolecules XXXX, XXX, XXX−XXX

frequencies above $\omega = 10^5$ rad/s, inertia effects become significant[33] and a simple, self-consistent correction scheme is used to account for that.[23] The influence of fluid inertia is determined by the high frequency viscosity.[34] Here we have estimated an effective high frequency viscosity of approximately 3 mPas in the regime $\omega = 10^5$–10^6 rad/s by extrapolating the $\omega < 10^5$ rad/s data for $G''(\omega)$ from mechanical measurements. We then correct the particle mean square displacement for inertia effects based on the theory of Hinch[35] developed for the motion of a sphere in a simple fluid with viscosity η. In a second iteration step, we again fit the resulting loss modulus and repeat this procedure several times. In our case the correction factor attains its smallest value of 0.7 for the shortest time analyzed $\tau = 5\cdot 10^{-7}$ s. A number of methods have been applied successfully to measure the particle mean square displacement, notably single particle tracking by microscopy, laser deflection and diffusing wave spectroscopy (DWS).[31,36,37] In this work, we have chosen DWS as the only technique that provides access to frequencies well above 10^4 rad/s.

The DWS technique is an extension of dynamic light scattering (DLS) to soft materials exhibiting strong multiple scattering.[38] The method allows to monitor the displacement of micrometer sized colloidal particles with subnanometer precision and on time scales as short as 10 ns. In recent years, significant progress has been made in development of the DWS approach and it has been successfully applied to study fluid and solid media for example wormlike micelles solutions[39−41] colloidal suspensions, gels, and biocolloids (yogurt and cheese), as well as ceramic slurries and green bodies.[42−45] In a DWS experiment, coherent laser light impinges on one side of a turbid sample and the intensity fluctuations of the light propagated through the sample are then analyzed either in transmission or backscattering geometry. A diffusion model is used to describe the propagation of photons across the sample. Analogous to traditional dynamic light scattering (DLS), for the case of noninteracting particles it is possible to express the measured intensity autocorrelation function (ICF) $g_2(\tau) - 1 = \langle I(t)\cdot I(t+\tau)\rangle/\langle I\rangle^2 - 1$ in terms of the mean square displacement of the scattering particle,

$$g_2(\tau) - 1 = \left[\int_0^\infty ds P(s)\exp(-(s/l^*)k^2\langle\Delta r^2(\tau)\rangle)\right]^2 \quad (9)$$

with $k = 2\pi n/\lambda$ being the wavenumber of light in a medium with refractive index n. $P(s)$ is the distribution of photon trajectories of length s in the sample and it can be calculated within the diffusion model taking into account the experimental geometry. For the case of transmission through a slab (plane-wave illumination), one obtains

$$g_2(t) - 1 = \left[\frac{(L/l^* + 4/3)\langle\sqrt{k_0^2\Delta r^2(t)}\rangle}{\sinh[(L/l^* + 4/3)\langle\sqrt{k_0^2\Delta r^2(t)}\rangle]}\right]^2 \quad (10)$$

The transport mean free path l^* characterizes the typical step length of the photon random walk given by the individual particle scattering properties and particle concentration; l^* can be determined independently by a comparison of the measured count rate to the one obtained with a sample of known l^*[46] and therefore enters the analysis as a constant parameter. Eq 10 numerically calculated the particle mean square displacement $\langle\Delta r^2(t)\rangle$ from the measured autocorrelation function $g_2(t)$.

In our experiments we added 0.5−1 wt % of titanium dioxide (TiO_2) particles (diameter 360 nm, LS instruments AG, Fribourg, Switzerland) to the NaHA solution. The sample was filled in standard glass cuvettes (Hellma) with a path length of 5 mm and a width of 10 mm. The temperature has been controlled within ±0.1 °C using a temperature control chamber. A 200 mW single frequency laser (Torus 532, Laser Quantum) operating at a wavelength $l = 532$ nm was used to illuminate a circular ground glass mounted on a two phase stepper motor. Putting a fast rotating diffuser in the optical path between laser and sample allows for more efficient ensemble averaging.[42] We collected the transmitted light coming from the ground glass and focused it onto the sample with a spot size diameter of roughly 5 mm. The scattered laser light was then collected using a single-mode optical fiber and single photon counting detector with high quantum efficiency and subsequently analyzed by a digital correlator. By numerical analysis using eq 10 we extracted the particle mean square displacement $\langle\Delta r^2(t)\rangle$ from the ICF typically over a range of values $g_2 = 0.01$−0.99. More details about the DWS device and data processing used here can be found in Oelschlaeger et al.[39]

Squeeze Flow. Oscillatory squeeze flow experiments were performed using a piezo-driven axial vibrator (PAV) customized at the Institute for Dynamic Material Testing (Ulm, Germany). General theory of squeeze flow is covered in standard textbooks of fluid mechanics.[47] The theory of the PAV as well as the mechanical and electronic setup used here are thoroughly discussed elsewhere[39,48,49] and therefore this is summarized here only briefly. In our squeeze flow experiments the samples are placed into a gap between two stainless steel plates. The lower plate is supported by a thin-walled quadratic copper tube carrying the piezo-elements, which exert the vibrational motion and pick-up the response signal. This lower part of the device is surrounded by a double-walled cylinder allowing for circulation of a thermostatting fluid and the sample temperature is controlled with an accuracy of ±0.1 °C. The upper boundary of the gap is a thick metal lid, which provides complete sealing of the fluid. The instrument operates at constant force amplitude and from the ratio of the dynamic displacement of the lower plate (amplitude ∼ 5 nm) with and without fluid the complex squeeze stiffness K^* of the fluid is obtained which is directly related to the complex shear modulus G^*:[49]

$$K^* = \frac{3\pi R4}{2d3}G^*/\left(1 + \frac{\rho\omega 2d2}{10G^*} + ...\right) \quad (11)$$

where ρ is the fluid density, R (here 10 mm) is the radius, and d is the height of the gap. The denominator in eq 11 is a series expansion taking into account the inertia of the fluid in the gap. The determination of G^* strongly depends on the exact knowledge of d, which is determined by calibration using Newtonian liquids with viscosities between 1 and 2000 mPas. Gap heights between 23 and 50 μm have been used here, corresponding to sample volumes between 100 and 200 μL. $G'(\omega)$ or $G''(\omega)$ values in the range from 0.1 to 10 kPa are accessible with the setup described here.

Rotational Rheometry. A rotational rheometer Thermo MARS II equipped with a cone−plate measuring cell (diameter $d_{CP} = 50$ mm, cone angle $\alpha_{cone} = 1°$) was used to perform steady as well as small amplitude oscillatory shear experiments covering the frequency range from 0.01 to 100 rad·s^{-1}. Strain sweep experiments performed prior to frequency sweeps ensure that the strain amplitude used was sufficiently small to provide a linear material response at all investigated frequencies. A solvent trap was used to avoid evaporation of the sample during the experiment.

RESULTS AND DISCUSSION

Comparison of Mechanical Rheometry and DWS Measurements and l_p Determination. Variations of the dynamic shear moduli G' and G'' with frequency as determined from mechanical and optical rheometry (after inertial correction) are given in Figure 1 for a 30 g/L NaHA solution in presence of 0.1 M NaCl at 20 °C. Generally, good agreement is found between mechanical and optical methods. For both techniques, the shapes of the relaxation spectra coincide very well over the whole frequency range, but in some cases absolute values of G' and G'' from DWS are higher (a factor of 2 at most) than the data from mechanical measurements. The most likely reason for this shift may be attributed to the aggregation of tracer particles which would reduce the mean square displacement and thus result in an apparent increase of G' and G''. Indeed, we have observed particle aggregation in NaHA solutions by visual inspection in an optical microscope, and typically these aggregates consist of 2−3 particles. Another possible explanation of this discrepancy may be due to interactions between the tracers and the surrounding medium. Compatibility can be shown by measuring samples with and

dx.doi.org/10.1021/bm4010436 | Biomacromolecules XXXX, XXX, XXX−XXX

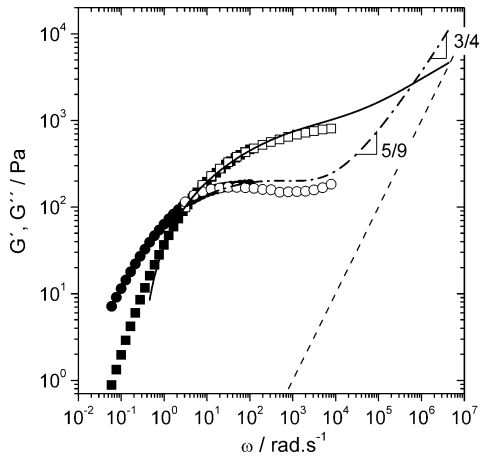

Figure 1. Dynamic shear moduli G' and G'' of a 30 g/L NaHA solution in presence of 0.1 M NaCl obtained from DWS after inertial correction (G' solid line, G'' dash-dotted line), oscillatory squeeze flow (G' open squares, G'' open circles), and rotational rheometry (G' closed squares, G'' closed circles) at T = 20 °C. The modulus of water $G'' = \omega\eta_s$ is included for reference (dashed line).

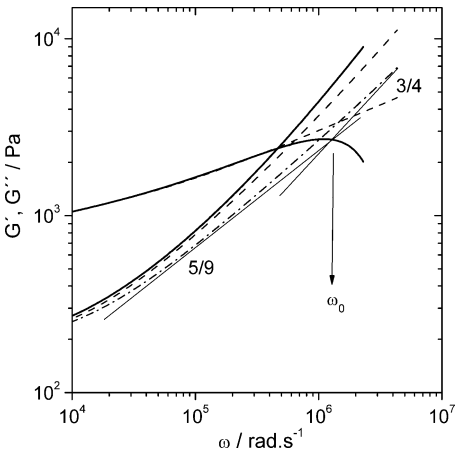

Figure 2. Dynamic shear moduli G' and $G''$of a 30 g/L NaHA solution in presence of 0.1 M NaCl obtained from DWS. Raw data (solid lines), after inertial correction (dashed lines), after subtracting water contribution (G'' only, dash-dotted lines).

without tracers mechanically, and we find no measurable differences within experimental error. Nevertheless, we cannot exclude that a small fraction of NaHA may interact with the tracer particles and therefore modify their mobility. Such interactions may have no effect on mechanical measurements but on DWS results. Concerning the variation of G' and G'', similar results were obtained for all systems investigated here. At low frequencies, $\omega < 1$ rad/s, the terminal flow regime with $G' \sim \omega^2$ and $G'' \sim \omega$ is observed and at intermediate frequencies, a well-developed quasi-plateau in G' (G' increases slightly with ω), which extends at least over two decades in frequency ($10^2 < \omega < 10^4$) is found. At high frequencies, $\omega > 10^4$ rad/s, the response is first dominated by the Rouse-Zimm modes with a scaling exponent G' or $G'' \sim \omega^{5/9}$ and at even higher frequencies, $\omega > 10^6$ rad/s, internal bending modes of single Kuhn segments dominate with $G'' \sim \omega^{3/4}$, as predicted theoretically[24,25] (see eq 6). However, G' does not scale as $G' \sim \omega^{3/4}$ in the frequency range investigated here, for the latter parameter the 3/4 variation will occur at higher frequencies. The characteristic rheological parameters: terminal relaxation time T_R and plateau modulus G_0 have been derived directly from the modulus curves. T_R is given by the inverse angular frequency corresponding to the first crossover of G' and G''. G_0 is determined as the value of the modulus G' at the frequency at which G'' has its local minimum, G''_{min}. The specific viscosity η_{sp} has been determined from steady shear measurements and is defined as $\eta_{sp} = ((\eta_0 - \eta_s)/\eta_s)$, where η_0 and η_s are the zero-shear viscosity and solvent viscosity, respectively. Variations of these parameters with NaHA concentration, ionic strength and temperature will be shown and discussed in the next section. Figure 2 represents variations of G' and G'' as a function of frequency obtained from DWS with and without inertia correction and after subtracting the solvent contribution. In order to obtain more reliable data in the ultrahigh frequency regime (up to ~10^7 rad/s), we applied a simple (self-consistent) correction scheme to account for inertial effects when the motion of the tracer particles changes from Brownian to ballistic. In particular, G' is strongly modified by this correction and the unphysical downward curvature at frequencies >10^6 rad/s is removed. The inertia correction also modifies G'' slightly, we have used this latter data set, after subtracting the solvent contribution ($-i\omega\eta_s$) from G'', to calculate l_p, because the $\omega^{3/4}$-scaling is more evident and extends over a broader frequency range in G'' than in G'. Here we should also mention that when $G''_{water} \approx G''_{sample}$ at high frequencies ($\omega \sim 10^6$ rad·s^{-1}); moduli data obtained after subtracting the water contribution scatter strongly and therefore no l_p determination is possible. This is the case for all solutions with hyaluronan concentration less than 10 g/L (dilute and unentangled semidilute regimes) but not for solutions at concentration $c > 10$ g/L corresponding to the semidilute entangled regime showing a much stronger viscoelastic behavior. Using eq 5, we found $\omega_0 = 1.2 \times 10^6$ rad·s^{-1} and $l_p = 7.5 \pm 1.5$ nm. Additionally, l_p has been determined from the absolute value of G^* in the $\omega^{3/4}$-scaling regime. We fit the function $G'' = k_{DWS}\cdot\omega^{3/4}$ to the experimental data and calculate l_p from the resulting k_{DWS} value according to eq 6. This equation requires a lateral drag coefficient $\zeta = 4\pi\eta_s/\ln(0.6\lambda/d_{NaHA})$. The characteristic length λ is set equal to the mesh size with $\lambda = (k_BT/G_0)^{1/3}$, η_s is the solvent viscosity, and for the NaHA diameter we insert d_{NaHA} = 0.7 nm[5]. This results in δ = 0.0047 N s/m^2 and $l_p = 7 \pm 1.4$ nm. Good agreement is found between the two l_p determination methods and both values are almost similar to those determined by Buhler et al.[17,18] using scattering techniques (l_p = 8−10 nm).

Effect of NaHA Concentration on the Specific Viscosity, η_{sp}, Relaxation Time, T_R, and Plateau Modulus, G_0, in the Presence of 0.1 M NaCl and in a Salt-Free System. Variations of η_{sp}, T_R, and G_0 in function of NaHA concentration in 0.1 M NaCl are given in Figure 3A−C, respectively. The entanglement concentration c_e, which characterizes the transition between the semidilute unentangled regime and the entangled regime, was determined to be c_e= 7 g/L, as indicated by an arrow in the three figures. For $c > c_e$, we found $\eta_{sp} \sim c^{4.0\pm0.2}$, $T_R \sim c^{2.0\pm0.3}$, and $G_0 \sim c^{2.5\pm0.3}$.

Similar exponents for the variation of the specific viscosity have been obtained by Krause et al.,[26] Fouissac et al.,[2] and Mo et al.[50] for NaHA solutions in presence of salt but also for neutral polymers.[51−53] This exponent is slightly higher than prediction for polyelectrolytes in the high salt limit[28] and solutions of neutral polymers in good solvent[29,54] where $\eta_{sp} \sim c^{3.75}$. For the relaxation time T_R (Figure 3B), we also found

dx.doi.org/10.1021/bm4010436 | Biomacromolecules XXXX, XXX, XXX−XXX

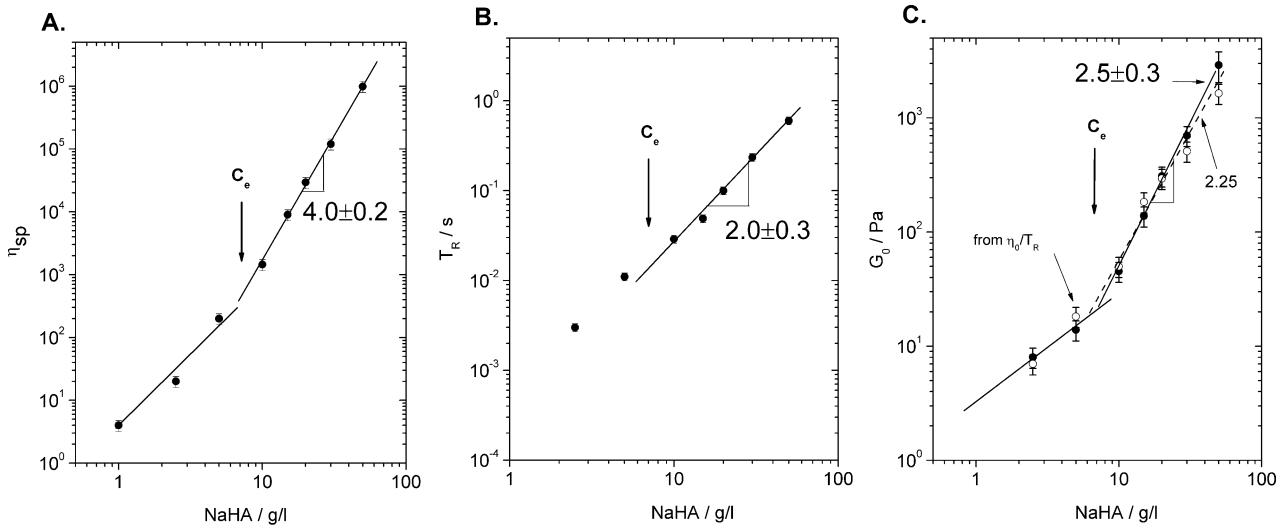

Figure 3. Variations of the specific viscosity, η_{sp} (A), relaxation time, T_R (B), and plateau modulus, G_0 (C) as a function of NaHA concentration in presence of 0.1 M NaCl. For (A) and (B), error bars are as large as the size of the different symbols. For (C), open circles are obtained from $G_0 \sim \eta_0/T_R$.

stronger concentration dependence than predicted theoretically ($T_R \sim c^{1.5}$). Similar deviations between experiment and theory are also reported for the low salt-limit in the entangled regime.[55,56] Also uncharged polymers in good solvent, which theory expects to have the same concentration dependences as polyelectrolytes with excess salt in entangled solution, exhibit slightly larger exponents than those predicted by reptation.[51,53] Figure 3C shows the variation of the plateau modulus G_0 as a function of concentration. G_0 has been determined directly from the relaxation curve as described in the previous section and also from the ratio of zero-shear viscosity and the relaxation time ($G_0 \approx \eta_0/T_R$). Good agreement is found between G_0 values obtained by the two methods. For this latter parameter, within experimental error, the scaling exponent agrees well with theoretical predictions for polyelectrolytes in high salt limit and neutral flexible polymers in good solvent ($G_0 \sim c^{2.25}$).[29] The reason for higher exponents observed for the concentration dependences of η_{sp} and T_R compared to theoretical predictions is most likely due to the formation of aggregates at higher NaHA concentration, which corresponds to an increase of the apparent molecular weight M_w and, thus, leads to stronger concentration dependence for these two parameters but not for G_0, which is independent of M_w. Aggregation is presumably due to the formation of hydrogen bonds between NaHA chains, which is more likely to happen at higher concentration.[7]

In salt free solutions exponents for concentration dependences of η_{sp}, T_R, and G_0 (not shown) are almost similar to those obtained in presence of salt. In the latter case, we found $\eta_{sp} \sim c^{3.9\pm0.2}$, $T_R \sim c^{2.0\pm0.2}$, and $G_0 \sim c^{2.3\pm0.3}$. Therefore, we conclude that at $c > c_e$ the presence of free ions in the solution due to high polysaccharide concentration already screens the electrostatic interactions strongly and the behavior is comparable to that of neutral polymers. Differences between salt free solutions and solutions in presence of excess salt reside in the absolute values of η_{sp}, T_R, and G_0. Upon addition of salt, η_{sp} and T_R decrease by a factor ~1.5 and G_0 by a factor ~1.3. This behavior may be attributed to a different conformation of the NaHA molecules due to the different electrostatic interactions, as shown by molecular dynamics simulations.[57]

Effect of Temperature on η_{sp}, T_R, and G_0. Increasing the temperature from 20 to 60 °C decreases η_{sp} by approximately a factor of 1.5 (η_0 by a factor of 3) and this corresponds to a strong increase in chain mobility. Figure 4 shows relaxation

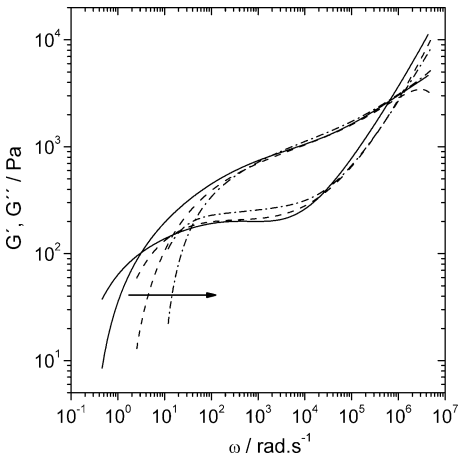

Figure 4. Dynamic shear moduli G' and G'' of a 30 g/L NaHA solution in presence of 0.1 M NaCl as a function of temperature obtained from DWS measurements: 20 °C (solid line), 40 °C (dashed line), 60 °C (dash-dotted line).

spectra for the system with NaHA 30 g/L in presence of 0.1m NaCl at three different temperatures 20, 40, and 60 °C obtained from DWS measurements. The terminal zone and the Maxwell relaxation frequency ω_R are strongly shifted toward higher frequencies, that is, the relaxation time T_R becomes faster when the temperature increases as expected. The activation energy E_A required for the relaxation of the system can be calculated from the slope of the semilogarithmic plot of T_R versus of $1/T$. We found an activation energy of 24 kJ/mol, this value is in good agreement with a previous study at a similar NaHA concentration.[58] We also observe that the plateau modulus G_0 is almost independent of temperature, which means that the mesh size of the entanglement network is essentially independent of temperature. The NaHA concentration dependences of η_{sp}, T_R, and G_0 at 60 °C are $\eta_{sp} \sim$

dx.doi.org/10.1021/bm4010436 | Biomacromolecules XXXX, XXX, XXX−XXX

$c^{3.8\pm0.2}$, $T_R \sim c^{2.0\pm0.2}$, and $G_0 \sim c^{2.3\pm0.3}$. The scaling exponents are essentially the same as obtained at 20 °C and there is no indication for a substantial change of polymer structure or conformation in this temperature range.

Persistence Length l_p. *Effect of NaHA Concentration on l_p in Presence of 0.1 M NaCl at $c > c_e$.* Before determining l_p for all NaHA solutions using MacKintosh's equation (eq 6), we have verified the validity of this latter approach by plotting the ratio of loss modulus and polysaccharide concentration as a function of frequency (Figure 5). At intermediate frequencies, $10^2 < \omega < 10^4$, this ratio depends on polysaccharide concentration but at higher frequencies, $\omega > 10^5$ rad/s, we found $G''/c \sim \omega^{3/4}$ and the curves for different concentrations coincide, that is, G'' depends linearly on concentration in this ω range. This result confirms that the high frequency modulus is indeed determined by the relaxation of individual chain segments, which is a prerequisite for the validity and applicability of eq 6. Figure 6 shows the variation of l_p as a function of NaHA concentration in the presence of 0.1 M NaCl, as determined from ω_0 (eq 5) and MacKintosh theory (eq 6). Good agreement is found between both methods and within experimental error l_p is almost independent of NaHA concentration with an average value of $l_p = 10 \pm 1.5$ nm. This value is similar to that obtained by Buhler et al.[18] in more dilute solutions using light scattering measurements, whereas significantly lower l_p values between 4 and 6 nm have been reported earlier based on small-angle X-ray scattering (SAXS) measurements.[5] The fact that the persistence length does not depend on the polysaccharide concentration is in good agreement with the OSF theory. Indeed, the intrinsic persistence length $l_{p,0}$ is concentration independent and only the electrostatic persistence length $l_{p,e}$ decreases with increasing polymer concentration. This latter parameter has been calculated using eqs 2 and 3; its variation with increasing NaHA is less than 0.1 nm in the concentration range investigated (see Table 2) and this is not detectable with our l_p determination method.

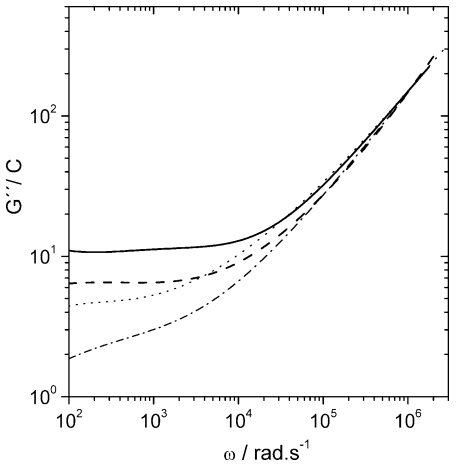

Figure 5. Variation of the ratio of the loss modulus and polysaccharide concentration in function of frequency obtained from DWS measurements. NaHA = 50 (solid line), 30 (dashed line), 15 (dotted line), and 10 g/L (dash-dotted line).

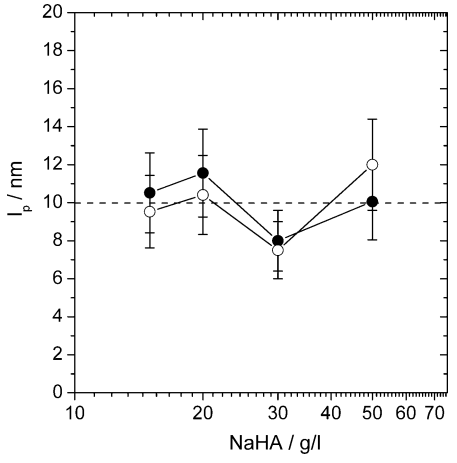

Figure 6. Variation of the persistence length l_p as a function of NaHA concentration in presence of 0.1 M NaCl obtained from Mackintosh theory (closed circles) and the crossover frequency of the $\omega^{5/9}$ and $\omega^{3/4}$ scaling regime (open circles).

Table 2. Theoretical Electrostatic Persistence Length, $l_{p,e}$ (Calculated with the OSF Model), Debye-Hückel Length, κ^{-1}, and Concentration of Free Monovalent Ions c_f

	salt free			NaCl 0.1 M		
NaHA (g/L)	c_f (mol/L)	κ^{-1} (nm)	$l_{p,e}$ (nm)	c_f (mol/L)	κ^{-1} (nm)	$l_{p,e}$ (nm)
15	0.0375	1.55	0.59	0.2375	0.62	0.09
20	0.0500	1.34	0.44	0.2500	0.60	0.09
30	0.0750	1.10	0.30	0.2750	0.57	0.08
50	0.1250	0.85	0.18	0.3250	0.53	0.07

Effect of Ionic Strength on l_p at $c > c_e$. Figure 7 shows the variation of the total persistence length $l_{p,T}$ measured

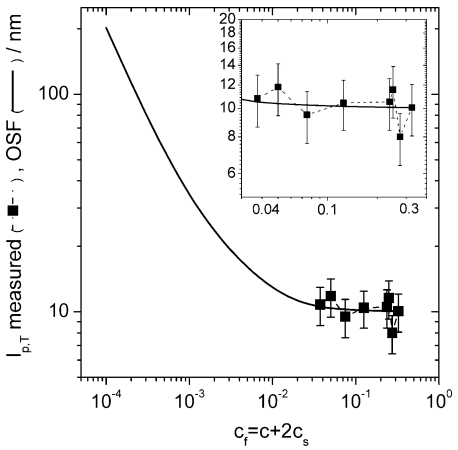

Figure 7. Variation of the total persistence length $l_{p,T}$ measured (closed squares) and calculated from OSF theory (solid line) as a function of the concentration of free monovalent ions c_f. Inset: enlarge.

experimentally using the MacKintosh equation and the variation predicted by the OSF theory $l_{p,OSF}$ as a function of the ionic strength c_f. For the OSF calculation, we approximate $l_{p,OSF} \sim l_{p,o} = 10$ nm for the solution with the highest polysaccharide concentration (50 g/L) and in the presence of 0.1 M NaCl; as for this sample, $l_{p,e}$ is negligibly small. We observe that $l_{p,T}$ experimental is almost independent of ionic strength within the experimental uncertainty throughout the experimental range ($0.0375 < c_f < 0.3250$ mol/L) investigated

dx.doi.org/10.1021/bm4010436 | Biomacromolecules XXXX, XXX, XXX–XXX

and is consistent with the small $l_{p,OSF}$ decrease (<0.6 nm) predicted by the OSF theory. The inset in Figure 7 emphasizes this result. Table 2 shows the electrostatic persistence length contribution $l_{p,e}$ calculated using eqs 5 and 6, the Debye–Hückel length k^{-1}, and the concentration of free monovalent ions c_f. For all salt-free solutions, $l_{p,e}$ is less than 0.6 nm, and this contribution is also too small to be detected with our experimental approach. The latter small contribution is due to the presence in a high quantity of free ions provided by the polysaccharide itself due to its high concentration. Therefore, the behavior with and without salt is almost similar.

Effect of Temperature on l_p at $c > c_e$. Figure 8 shows the variation of the persistence l_p as a function of temperature (20, 40, and 60 °C) for a 30 g/L NaHA solution in presence of 0.1 M NaCl. Regardless of the l_p determination method, we found that l_p is independent of temperature within experimental error. Similar results have been obtained experimentally[59] and from molecular modeling.[19] In the latter study, authors found a moderate l_p decrease from 7.5 to 5.5 nm when increasing the temperature from 25 to 100 °C, respectively. This slight decrease of the stiffness is probably due to a destabilization or breaking of the intrachain hydrogen bonds and is also demonstrated by the decrease of the zero-shear viscosity when temperature increases, whereas the specific viscosity is independent of temperature.

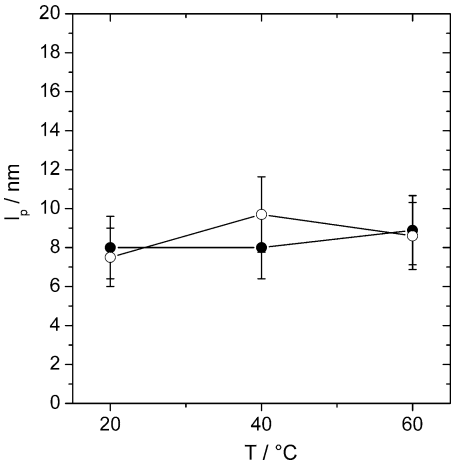

Figure 8. Variation of the persistence length l_p as a function of temperature in presence of 0.1 M NaCl obtained from Mackintosh theory (closed circles) and the crossover frequency of the $\omega^{5/9}$ and $\omega^{3/4}$ scaling regime (open circles).

CONCLUSIONS

In this work, we have used high frequency mechanical rheology and DWS to characterize the linear viscoelastic properties of NaHA solutions in a frequency range from 10^{-1} to 10^{7} rad·s^{-1}. The persistence length l_p of NaHA solutions has been determined directly from rheological measurements for the first time, and we have found $l_p = 10 \pm 1.5$ nm. This value is independent of NaHA concentration and ionic strength as expected from OSF theory in the semidilute entangled regime investigated here. Furthermore, l_p is also independent of temperature. Experimental scaling exponents for concentration dependence of specific viscosity η_{sp} and relaxation time T_R show slightly higher values than theoretically predicted for polyelectrolytes in the high salt limit and neutral polymer in good solvent, whereas for the plateau modulus G_0, the scaling exponent agrees well with theoretical predictions. This behavior is presumably due to the formation of aggregates in the high concentrated NaHA regime leading to an increase of the apparent M_w.

AUTHOR INFORMATION

Corresponding Author

*E-mail: claude.oelschlaeger@kit.edu.

Notes

The authors declare no competing financial interest.

ACKNOWLEDGMENTS

The authors thank Kristoffer Tømmeraas (Novozymes A/S, Denmark) for providing the hyaluronan.

REFERENCES

(1) Fouissac, E.; Milas, M.; Rinaudo, M.; Borsali, R. *Macromolecules* **1992**, *25*, 5613–5617.
(2) Fouissac, E.; Milas, M.; Rinaudo, M. *Macromolecules* **1993**, *26*, 6945–6951.
(3) Rinaudo, M.; Milas, M.; Jouon, N.; Borsali, R. *Polymer* **1993**, *34*, 3710–3715.
(4) Roure, I.; Rinaudo, M.; Milas, M. *Ber. Bunsenges. Phys. Chem.* **1996**, *100*, 703–706.
(5) Cleland, R. L. *Biopolymers* **1984**, *23*, 647–666.
(6) Rinaudo, M.; Roure, I.; Milas, M. *Int. J. Polym.* **1999**, *5*, 277–287.
(7) Esquenet, C.; Buhler, E. *Macromolecules* **2002**, *35*, 3708–3716.
(8) Hayashi, K.; Tsutsumi, K.; Nakajima, F.; Norisuye, T.; Teramoto, A. *Macromolecules* **1995**, *28*, 3824–3830.
(9) Takahashi, R.; Kubota, K.; Kawada, M.; Okamoto, A. *Biopolymers* **1999**, *50*, 87–98.
(10) Tsutsumi, K.; Norisuye, T. *Polym. J.* **1998**, *30*, 345–349.
(11) Cowman, M. K.; Matsuoka, S. In *Hyaluronan*; Kennedy, J. F., Phillips, G. O., Williams, P. A., Eds.; Woodhead: Cambridge, 2002; pp 75–78.
(12) Gamini, A.; Paoletti, S.; Zanetti, F. Chain Rigidity of Polyuronates: Static Light Scattering of Aqueous Solutions of Hyaluronate and Alginate. In *Laser Light Scattering in Biochemistry*; Harding, S. E., Satelle, D. B., Bloomfield, V. A., Eds.; Royal Society of Chemistry: Cambridge, 1992; pp 294–311.
(13) Mendichi, R.; Soltes, L.; Schieroni, A. G. *Biomacromolecules* **2003**, *4*, 1805–1810.
(14) Milas, M.; Roure, I.; Berry, G. C. *J. Rheol.* **1996**, *40*, 1155–1166.
(15) Berriaud, N.; Milas, M.; Rinaudo, M. Characterization and Properties of Hyaluronic Acid (Hyaluronan). In *Polysaccharides in Medicine and Technology*; Severian, D., Ed.; Marcel Dekker: New York, 1998; pp 313–334.
(16) Ghosh, S.; Li, X.; Reed, C. E.; Reed, W. F. *Biopolymers* **1990**, *30*, 1101–1112.
(17) Buhler, E.; Boué, F. *Eur. Phys. J. E* **2003**, *10*, 89–92.
(18) Buhler, E.; Boué, F. *Macromolecules* **2004**, *37*, 1600–1610.
(19) Haxaire, K.; Braccini, I.; Milas, M.; Rinaudo, M.; Pérez, S. *Glycobiology* **2000**, *10*, 587–594.
(20) Manning, G. S. *J. Chem. Phys.* **1969**, *51*, 924–933.
(21) Odijk, T. *J. Polym. Sci., Polym. Phys. Ed.* **1977**, *15*, 477–483.
(22) Skolnick, J.; Fixman, M. *Macromolecules* **1977**, *10*, 944–948.
(23) Willenbacher, N.; Oelschlaeger, C.; Schopferer, M.; Fischer, P.; Cardinaux, F.; Scheffold, F. *Phys. Rev. Lett.* **2007**, *99* (6), 068302.
(24) Morse, D. C. *Phys. Rev. E* **1998**, *58* (2), R1237–R1240.
(25) Gittes, F.; MacKintosh, F. C. *Phys. Rev. E* **1998**, *58* (2), R1241–R1244.
(26) Krause, W. E.; Bellomo, E. G.; Colby, R. H. *Biomacromolecules* **2001**, *2*, 65–69.
(27) Milas, M.; Rinaudo, M. In *Characterization and Properties of Hyaluronic Acid (Hyaluronan) Polysaccharides: Structural Diversity and Functional Versatility*; Dimitriu, S., Ed.; Dekker: New York, 2004; pp 535–549, ISBN 0824754808.

(28) Dobrynin, A. V.; Colby, R. H.; Rubinstein, M. *Macromolecules* **1995**, *28*, 1859−1871.
(29) de Gennes, P. G. *Scaling Concepts in Polymer Physics*; Cornell University Press: Ithaca, NY, 1979.
(30) Mason, T. G.; Weitz, D. A. *Phys. Rev. Lett.* **1995**, *74*, 1250−1253.
(31) Mason, T. G.; Ganesan, K.; van Zanten, J. H.; Wirtz, D.; Kuo, S. C. *Phys. Rev. Lett.* **1997**, *79*, 3282−3285.
(32) von Berlepsch, H.; Harnau, L.; Reineker, P. *J. Phys. Chem. B* **1998**, *102*, 7518−7522.
(33) Weitz, D. A.; Pine, D. J.; Pusey, P. N.; Though, R. J. A. *Phys. Rev. Lett.* **1989**, *63*, 1747−1750.
(34) Ladd, A. J. C.; Gang, H.; Zhu, J. X.; Weitz, D. A. *Phys. Rev. Lett.* **1995**, *74*, 318−321.
(35) Hinch, E. *J. Fluid Mech.* **1975**, *72*, 499−511.
(36) Xu, J.; Tseng, Y.; Carriere, C. J.; Wirtz, D. *Biomacromolecules* **2002**, *3*, 92−99.
(37) Gardel, M. L.; Valentine, M. T.; Crocker, J. C.; Bausch, A. R.; Weitz, D. A. *Phys. Rev. Lett.* **2003**, *91*, 158302.
(38) Maret, G.; Wolf, P. E. *Z. Phys. B: Condens. Matter Quanta* **1987**, *65*, 409−413.
(39) Oelschlaeger, C.; Schopferer, M.; Scheffold, F.; Willenbacher, N. *Langmuir* **2009**, *25*, 716−723.
(40) Oelschlaeger, C.; Suwita, P.; Willenbacher, N. *Langmuir* **2010**, *26* (10), 7045−7053.
(41) Galvan-Miyoshi, J.; Delgado, J.; Castillo, R. *Eur. Phys. J. E* **2008**, *26*, 369−377.
(42) Zakharov, P.; Cardinaux, F.; Scheffold, F. *Phys. Rev. E* **2006**, *73*, 011413.
(43) Scheffold, F.; Schurtenberger, P. *Soft Mater.* **2003**, *1*, 139−165.
(44) Schurtenberger, P.; Stradner, A.; Romer, S.; Urban, C.; Scheffold, F. *Chimia* **2001**, *55* (3), 155−159.
(45) Heinemann, C.; Cardinaux, F.; Scheffold, F.; Schurtenberger, P.; Escher, F.; Conde-Petit, B. *Carbohydr. Polym.* **2004**, *55* (2), 155−161.
(46) Kaplan, P. D.; Kao, M. H.; Yodh, A. G.; Pine, D. J. *Appl. Opt.* **1993**, *32*, 3828−3836.
(47) Bird, R. B.; Armstrong, R. C.; Hassager, O. *Dynamics of Polymeric Liquids, Fluid Dynamics*, 2nd ed.; Wiley: New York, 1987; Vol. *1*, p 784.
(48) Crassous, J. J.; Regisser, R.; Ballauff, M.; Willenbacher, N. *J. Rheol.* **2005**, *49*, 851−863.
(49) Kirschenmann L. *Ph.D. Thesis, Institut fur Dynamische Materialprufung*, University of Ulm, 2003.
(50) Mo, Y.; Takaya, T.; Nischinari, K.; Kubota, K.; Okamoto, A. *Biopolymers* **1999**, *50*, 23−34.
(51) Pearson, D. S. *Rubber Chem. Technol.* **1987**, *60*, 439−496.
(52) Takahashi, Y.; Isono, Y.; Noda, I.; Nagasawa, M. *Macromolecules* **1985**, *18*, 1002−1008.
(53) Berry, G. C.; Fox, T. G. *Adv. Polym. Sci.* **1968**, *5*, 261−357.
(54) Colby, R. H.; Rubinstein, M.; Daoud, M. *J. Phys. II* **1994**, *4*, 1299−1310.
(55) Boris, D. C.; Colby, R. H. *Macromolecules* **1998**, *31*, 5746−5755.
(56) Krause, W. E.; Tan, J. S.; Colby, R. H. *J. Polym. Sci., Part B: Polym. Phys.* **1999**, *37*, 3429−3437.
(57) Carrillo, J. A. Y.; Dobrynin, A. V. *Macromolecules* **2011**, *44*, 5798−5816.
(58) Charlot, A.; Auzély-Velty, R. *Macromolecules* **2007**, *40*, 9555−9563.
(59) Haxaire, K.; Buhler, E.; Milas, M.; Perez, S.; Rinaudo, M. In *Hyaluronan*; Kennedy, J. F., Phillips, G. O., Williams, P. A., Eds.; Woodhead Pub.: Cambridge, U.K., 2002; Vol. *1*, p 37.